

Article

Novel Ionic Liquid Synthesis of Bimetallic Fe–Ru Catalysts for the Direct Hydrogenation of CO₂ to Short Chain Hydrocarbons

Marina Maddaloni ^{1,2} , Ander Centeno-Pedraza ³ , Simone Avanzi ¹, Nayan Jyoti Mazumdar ³, Haresh Manyar ³ and Nancy Artioli ^{1,*} 

¹ CEEP Laboratory, Department of Civil Engineering, Architecture, Territory, Environment and Mathematics, University of Brescia, Via Branze 38, 25123 Brescia, Italy; marina.maddaloni@unibs.it (M.M.); s.avanzi002@studenti.unibs.it (S.A.)

² Consorzio Interuniversitario Nazionale per la Scienza e Tecnologia dei Materiali (INSTM), University of Brescia, Via Branze 38, 25123 Brescia, Italy

³ School of Chemistry and Chemical Engineering, Queen's University Belfast, David-Keir Building, Stranmillis Road, Belfast BT9 5AG, UK; a.centeno@qub.ac.uk (A.C.-P.); nmazumdar01@qub.ac.uk (N.J.M.); h.manyar@qub.ac.uk (H.M.)

* Correspondence: nancy.artioli@unibs.it

Abstract: The selective hydrogenation of CO₂ for the production of net-zero fuels and essential chemical building blocks is a promising approach to combat climate change. Key to this endeavor is the development of catalysts with high activity and selectivity for desired hydrocarbon products in the C₂–C₅ range. The process involves a two-step reaction, starting with the reverse water-gas shift (RWGS) reaction and proceeding to the Fischer–Tropsch reactions under high pressure. Understanding the catalyst features that control the selectivity of these pathways is crucial for product formation, as well as identifying morphological changes in the catalysts during the reaction to optimize their performance. In this study, an innovative method for synthesizing iron–ruthenium bimetallic catalysts is introduced, capitalizing on the synergistic effects of these metals as active phases. This method leverages ionic liquids as solvents, allowing for the precise and uniform distribution of active metal phases. Advanced characterizations and extensive catalytic tests have demonstrated that the use of ionic liquids outperformed traditional colloid-based techniques, resulting in superior selectivity for target hydrocarbons. The success of this inventive approach not only advances the field of CO₂ hydrogenation catalysis, but also represents a significant stride towards sustainable e-fuel production.

Keywords: CO₂ hydrogenation; iron ruthenium; hydrocarbons; ionic liquid solvent



Citation: Maddaloni, M.; Centeno-Pedraza, A.; Avanzi, S.; Mazumdar, N.J.; Manyar, H.; Artioli, N. Novel Ionic Liquid Synthesis of Bimetallic Fe–Ru Catalysts for the Direct Hydrogenation of CO₂ to Short Chain Hydrocarbons. *Catalysts* **2023**, *13*, 1499. <https://doi.org/10.3390/catal13121499>

Academic Editor: Chunxi Li

Received: 11 October 2023

Revised: 28 November 2023

Accepted: 5 December 2023

Published: 7 December 2023



Copyright: © 2023 by the authors. Licensee MDPI, Basel, Switzerland. This article is an open access article distributed under the terms and conditions of the Creative Commons Attribution (CC BY) license (<https://creativecommons.org/licenses/by/4.0/>).

1. Introduction

In recent years, the scientific community's efforts have increasingly shifted towards the development of net zero carbon technologies aimed at minimizing CO₂ emissions into the atmosphere. The aim of the European Union is to achieve a 45% reduction in net CO₂ emissions by 2030 compared to the levels estimated in 2010, with the goal of reaching net zero emissions by 2050. In this way, the limitation of global warming to less than 2 °C annually is estimated [1].

These goals can be achieved through significant measures to mitigate CO₂ emissions, spanning various sectors, including industry, energy, and transportation. In particular, the transport sector is responsible for more than 18% of greenhouse gas emissions [2] due to the use of petrol and diesel-based vehicles, and therefore represents a sector in which alternative measures are urgently needed. Nowadays, among the cleanest alternatives to vehicles conventional fuels, Liquefied Petroleum Gas (LPG) stands out [3], as it offers distinct advantages, and represents the bridge between the fuels that are currently most

The synergistic effect of bimetallic Ru and Fe active sites on catalyst performance is debated in the literature, and is related to their bimetallic interface and surface structural characteristics. Preparing iron catalysts typically involves saturating a support with two metal salt precursors. However, this may not ensure uniform alloy nanoparticle formation. Bimetallic catalysts often contain iron and ruthenium phases as alloys and separate metal nanoparticles [10]. Reductions in alumina-impregnated salts generate Fe/Ru alloys and isolated iron and ruthenium nanoparticles, resulting in metal diversity in various phases and oxidation states. This heterogeneity may explain the variable catalytic activity, notably in how ruthenium affects iron-based catalysts in Fischer–Tropsch (FT) reactions. Some studies suggest Ru enhances CO₂ conversion, shifting product distribution to heavier hydrocarbons [12], while others report no significant Ru impact on activity or selectivity [13].

It is paramount to achieve the precise and consistent synthesis of stable metal nanoparticles (MNPs) to exert control over the activity of bimetallic catalysts. To address this, we have introduced a novel approach for synthesizing Fe/Ru bimetallic catalysts using ionic liquid solvents. Ionic liquids (ILs), functioning as nanosynthetic templates [14], enhance MNP stability due to their high ionic charge, strong polarity, elevated dielectric constant, and supramolecular network. Unlike traditional solvents, which mainly consist of neutral molecules, ILs comprise solely charged species, whether these be organic or inorganic ions. They offer new prospects for sustainable and environmentally friendly chemistry, serving as alternatives to volatile organic solvents [15,16].

The existing literature has emphasized the utility of ionic liquids for nanoparticle stabilization when synthesizing Ru monometallic nanoparticles and Fe₂O₃ nanoparticles within the ionic liquid [BmIm][BF₄], without requiring additional stabilizers or capping agents. These nanoparticles exhibit an extraordinarily small and uniform size, typically ranging from 1.5 to 2.5 nm [14].

In continuation of our group's interest in the development of renewable e-fuel technologies and environmental catalysis [17–25], we have developed a novel synthesis method for Fe/Ru bimetallic catalysts using ionic liquids [BmIm][PF₆] and [BmIm][BF₄] as novel solvents for BiMetallic NPs (BMNPs) synthesis. Our method leverages readily available metal carbonyl precursors, facilitating scalability to encompass a wide array of other metal carbonyl complexes. Metal carbonyls are attractive starting materials for nanosynthesis due to their high purity. Furthermore, we utilize readily available low-cost ionic liquids, which are produced in substantial quantities.

Our developed catalyst synthesis method is easily reproducible, and viable for suitable scaling up. The resulting nanoparticles can be easily separated from the ionic liquid, and the ionic liquid can be reused. The nanoparticles can be redispersed in various polar solvents such as acetone, methanol and ethanol, and impregnated onto the final support material, in our case alumina.

The efficacy of our novel synthesis method was assessed through extensive catalytic experiments carried out under diverse conditions, examining its impact on the newly synthesized bimetallic NPs on the catalytic performance in CO₂ hydrogenation to short-chain hydrocarbons. The outcomes of these tests have revealed that employing ionic liquids outperformed conventional colloid-based approaches, yielding enhanced conversion rates and higher selectivity towards short-chain hydrocarbons. This achievement underscores the potential of using our innovative methodology in expanding the utilization of ILs for tailored NP synthesis catalysis. Notably, it shows promise in applications involving reactions that are particularly sensitive to metal–metal interactions, such as CO₂ hydrogenation for sustainable e-fuel production.

2. Results and Discussion

The morphological characteristics of the catalysts synthesized through colloidal and ionic liquid methods are detailed in Table 1.

Table 1. Catalysts summary table.

Catalyst Name	Fe:Ru Ratio	Total Metal Amount (%)	BET		XRF (wt. %)
			Surface Area (m ² /g)	Pore Size (Å)	
1 wt.% Fe/Al ₂ O ₃ (COL)	-	1	109.41	86.84	0.95
1 wt.% Ru/Al ₂ O ₃ (COL)	-	1	105.16	86.40	1.4
1 wt.% Fe–Ru 1:1/Al ₂ O ₃ (COL)	1:1	1	88.46	84.95	Fe 0.57 Ru 0.67
1 wt.% Fe–Ru 3:1/Al ₂ O ₃ (COL)	3:1	1	109.44	86.81	Fe 0.7 Ru 0.27
1 wt.% Fe–Ru 9:1/Al ₂ O ₃ (COL)	9:1	1	90.17	87.95	Fe 1.13 Ru 0.10
4 wt.% Fe–Ru 1:1/Al ₂ O ₃ (COL)	1:1	4	90.17	82.21	Fe 1.46 Ru 1.76
1 wt.% Fe/Al ₂ O ₃ (IL)	-	1	99.32	91.02	0.93
1 wt.% Ru/Al ₂ O ₃ (IL)	-	1	81.61	99.83	1.44
1 wt.% Fe–Ru 1:1/Al ₂ O ₃ (IL)	1:1	1	86.14	97.34	Fe 0.6 Ru 0.7
1 wt.% Fe–Ru 3:1/Al ₂ O ₃ (IL)	3:1	1	93.79	88.08	Fe 0.98 Ru 0.29
1 wt.% Fe–Ru 9:1/Al ₂ O ₃ (IL)	9:1	1	112.23	91.72	Fe 0.88 Ru 1
4 wt.% Fe–Ru 1:1/Al ₂ O ₃ (IL)	1:1	4	51.22	108.64	Fe 2 Ru 2

XRF analysis has indicated that both methods successfully achieved catalysts with metal loading amounts close to the theoretical values. In the case of bimetallic samples with 1% *w/w* loading prepared using the ionic liquid solvent, their surface areas closely resemble those of samples prepared via the colloidal method, ranging from 88 to 95 m²/g, with pore sizes spanning 86–92 Å. However, as the metal loading was increased from 1 to 4%, the surface area decreased to 51 m²/g, accompanied by an increase in the average pore diameter to 109 Å.

To gain deeper insights into the impact of the new synthetic method on the catalyst's structure, especially concerning the Fe–Ru ratio, we have first compared the XRD patterns of the fresh catalysts.

In Figure 1a, we compare three fresh catalysts obtained using the colloidal method, all with identical total metal loadings (1%—see Table 1) but varying in their Fe:Ru ratios (1:1, 3:1 and 9:1), while in Figure 1b we illustrate the same comparison between the three bimetallic catalysts (1:1, 3:1 and 9:1) and the monometallic catalysts (1 wt. % Fe/Al₂O₃) obtained via the ionic liquid procedure.

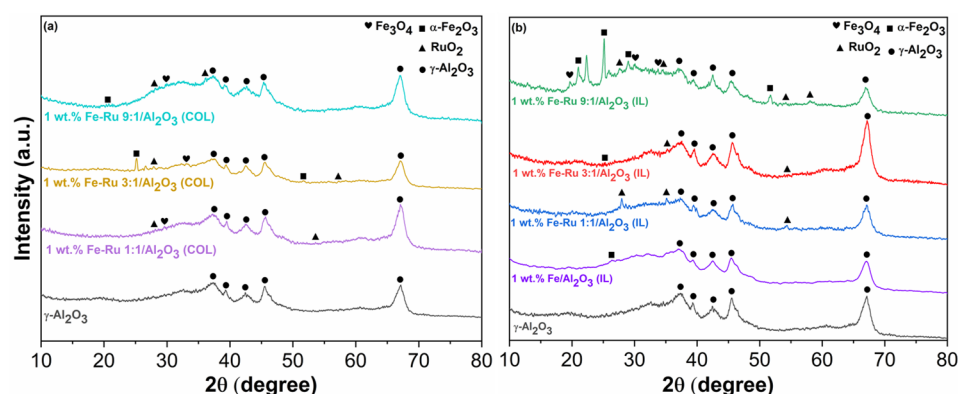


Figure 1. (a) XRD patterns of fresh catalysts prepared with colloidal method: 1 wt.% Fe–Ru 1:1/Al₂O₃ (COL), 1 wt.% Fe–Ru 3:1/Al₂O₃ (COL) and 1 wt.% Fe–Ru 9:1/Al₂O₃ (COL), compared with the pure γ -Al₂O₃. (b) XRD patterns of fresh catalysts prepared with ionic liquid method: 1 wt.% Fe/Al₂O₃ (IL), 1 wt.% Fe–Ru 1:1/Al₂O₃ (IL), 1 wt.% Fe–Ru 3:1/Al₂O₃ (IL) and 1 wt.% Fe–Ru 9:1/Al₂O₃ (IL), compared with the pure γ -Al₂O₃.

In both cases (IL and COL), the low percentage of metal loading does not allow a clear display of all peaks associated with the presence of iron species. However, the peaks corresponding to the scattering of (012) and (116) planes of α Fe₂O₃ [26] are visible for both

types of catalysts obtained by the two methods, in particular for the catalysts with an Fe–Ru ratio 3:1. These peaks in these samples enable the calculation of the crystallite average size (D_F), which is indicative of nanoparticle dimensions, using the Scherer's equation [26]:

$$D_F = \frac{K\lambda}{\beta \cos \theta}$$

where K is the Scherer constant (0.9), λ is the wavelength of the radiation (0.15406 nm), θ is the angle of scattering and β is the FWHM (Full Width at Half Maximum).

The obtained results (30.12 nm for 1 wt.% Fe–Ru 3:1/ Al_2O_3 (COL) and 22 nm for 1 wt.% Fe–Ru 3:1/ Al_2O_3 (IL)) reveal how the type of treatment employed for catalyst synthesis influenced the resulting nanoparticles, which were smaller in the case of the IL method, possibly justifying greater activity in the FT step. However, in both cases, the size of the nanoparticles falls within the expected range [27,28]. This difference is also clearly discernible through a direct comparison of the diffraction patterns between the two catalyst types. In fact, upon examining Figure 1b alongside Figure 1a, it becomes evident that in the case of ionic liquids, peaks associated with $\alpha\text{Fe}_2\text{O}_3$ are more distinctly resolved. Moreover, it is noteworthy that the intensity of these peaks increases proportionally with the rise in the Fe percentage in the catalysts, transitioning from the Fe:Ru ratio of 1:1 to 9:1. In both instances, even more than in the case of iron species, both metallic Ru and RuO_x are either undetected or identified as low-intensity peaks, even in the XRD pattern of the ionic liquid samples, which are generally better resolved. This observation may stem not only from the low total metal loading, but also suggests the high dispersion of Ru species on the support.

The objective of our study is to compare the catalytic activity of catalysts prepared using different methods (colloidal and ionic liquid). For this purpose, Figure 2 displays the TPR profiles of the catalysts with different Fe–Ru ratios prepared with the colloidal (Figure 2a) and ionic liquid methods (Figure 2b).

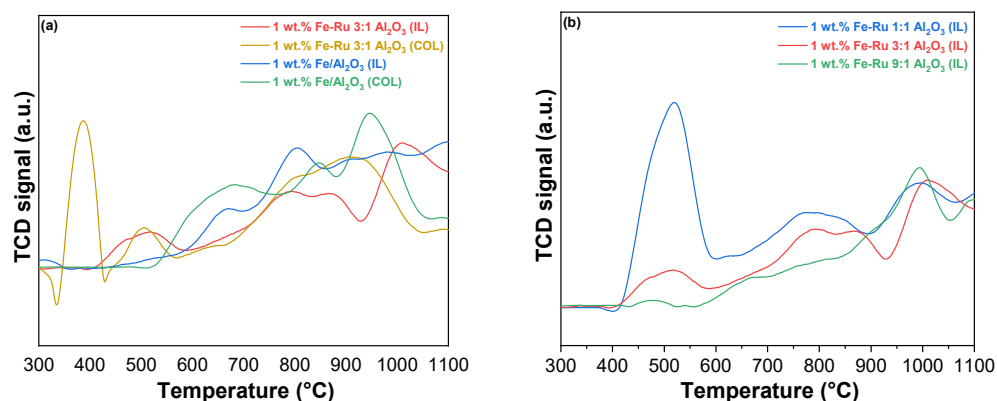


Figure 2. (a) H_2 -TPR profiles of catalysts 1 wt.% Fe–Ru 3:1/ Al_2O_3 (COL) (in yellow), 1 wt.% Fe–Ru 3:1/ Al_2O_3 (IL), 1 wt.% Fe/ Al_2O_3 (COL), and 1 wt.% Fe/ Al_2O_3 (IL). (b) H_2 -TPR profiles of catalysts, 1 wt.% Fe–Ru 1:1/ Al_2O_3 (IL), 1 wt.% Fe–Ru 3:1/ Al_2O_3 (IL) and 1 wt.% Fe–Ru 9:1/ Al_2O_3 (IL).

The H_2 -TPR profiles of Fe_2O_3 - RuO_2 catalysts prepared using different methods (colloidal and ionic liquid) are portrayed in Figure 2 to investigate the difference in the redox performance according to the different reduction profiles with respect to reduction temperature and amount of H_2 consumed for reduction.

In Figure 2a, the catalysts 1 wt.% Fe–Ru 3:1/ Al_2O_3 (COL) and 1 wt.% Fe–Ru 3:1/ Al_2O_3 (IL) are reported. In both catalysts, the two reduction peaks associated with Fe_2O_3 are observed. The low-temperature reduction peak, which appeared at approximately 380 °C, was assigned to the reduction of Fe_2O_3 to Fe_3O_4 , and the high-temperature reduction peak starting at 620 °C can be assigned to the further reduction of Fe_3O_4 to FeO and Fe⁰.

The reduction peaks belonging to Fe_2O_3 in RuO_2 - Fe_2O_3 catalysts are shifted to lower temperatures compared with what has been reported in the literature for the pure Fe_2O_3

catalyst [28]. Moreover, a low-temperature (500 °C) reduction peak is observed in these bimetallic catalysts. This peak could be attributed to the easier reduction of RuO₂ species. This result demonstrates that the addition of RuO₂ accelerated the Fe species reduction, simultaneously revealing the occurrence of hydrogen spillover from Ru atoms to Fe₂O₃ [28]. Namely, the positive impact of Ru species on the reduction of Fe species illustrates the existence of cooperativity between RuO₂ and Fe₂O₃, which could greatly enhance the reduction property. This result was correlated to the improved catalytic performance. It is noteworthy that a distinct difference between the catalysts obtained using the two different methods is evident even at low temperatures (300 °C < T < 470 °C). Specifically, in the case of the colloidal catalyst, the peak associated with the reduction of Ru⁴⁺ to Ru⁰ is highly pronounced [22,29,30]. However, this peak nearly disappears in the case of the IL catalyst. This can be attributed to the presence of a more isolated ruthenium metal phase in the case of catalyst 1 wt.% Fe–Ru 3:1/Al₂O₃ (COL), as opposed to the other sample, where the two metals exhibit a more pronounced synergistic effect due to their closer proximity. Notably, the reduction at 500 °C, attributed to the reduction of RuO₂ associated with Fe [31], is more prominent in the ionic liquid catalyst.

From the comparison of the reduction profiles among the three IL catalysts with different Fe:Ru ratios (Figure 2b), it is evident that the peak related to Ru⁴⁺/Ru⁰ reduction (T = 470 °C) diminishes when the reduction of ruthenium takes precedence over iron in the catalyst. Furthermore, regardless of the varying ratios of the two metals in the samples, all the distinctive characteristic peaks observed in the colloidal system remain clearly defined. Thus, ionic liquid synthesis improves the reducibility by increasing the cooperativity between Fe and Ru species due to their closer proximity [31,32].

The morphologies of the bimetallic Fe–Ru/Al₂O₃ catalysts prepared using colloidal and ionic liquid methods with varying Fe:Ru ratios were characterized using SEM analysis (Figure 3).

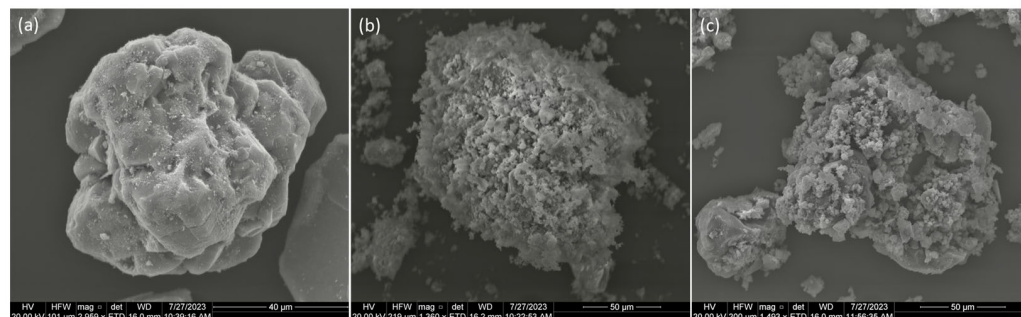


Figure 3. SEM images of various Fe–Ru/Al₂O₃ catalysts synthesized using colloidal and ionic liquid methods: (a) 4 wt.% Fe–Ru 7:1/Al₂O₃ (COL), (b) 1 wt.% Fe–Ru 1:1/Al₂O₃ (IL), and (c) 4 wt.% Fe–Ru 1:1/Al₂O₃ (IL).

It can be seen from Figure 3a that the particles of the catalyst prepared using the colloidal method, 4 wt.% Fe–Ru 7:1/Al₂O₃ (COL), are large with an irregular morphology and a smooth surface. In contrast, the catalyst particles prepared using the ionic liquid method, for instance, 1 wt.% Fe–Ru 1:1/Al₂O₃ (IL) (Figure 3b) and 4 wt.% Fe–Ru 1:1/Al₂O₃ (IL) (Figure 3c), show agglomerates of numerous smaller nanoparticles, with irregular but rough surfaces.

Finally, activity experiments at a single temperature of 320 °C and GHSV of 5400 mL/h/gcat, and at two pressures of 20 bar (Figures 4 and 5) and 6 bar (Figure 6), were carried out for each synthesized catalyst. High pressure test conditions are closer to industrial settings, where high pressures are often employed, and low pressures have been investigated for screening purpose. Although CH₄ is the primary expected product at these conditions, the information gathered via these experiments is invaluable for comparing the activity and selectivity of the catalysts prepared via the two different synthetic routes [11].

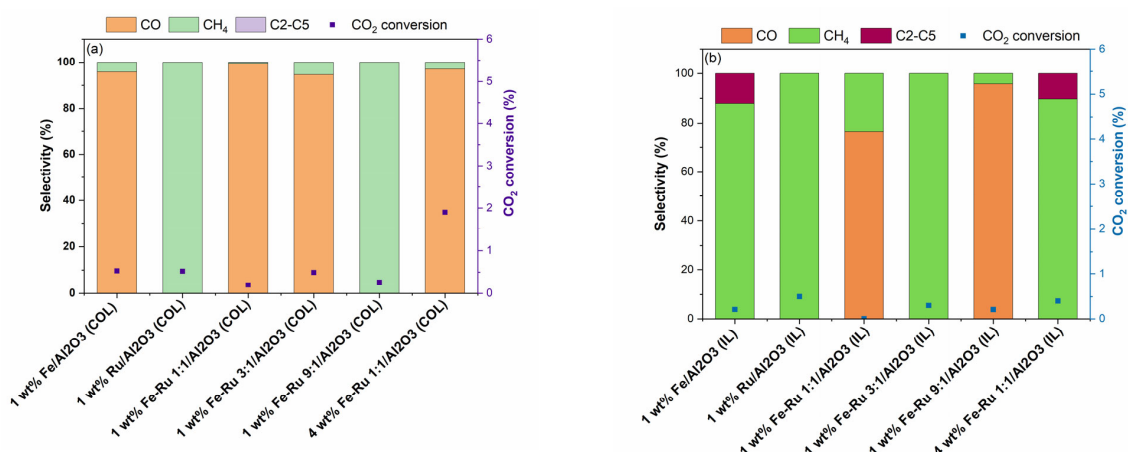


Figure 4. (a) CO₂ conversion (%) and selectivity for the colloidal catalysts at 20 bar and 45 mL/min corresponding to a space velocity of 5400 mL/h/gcat. (b) CO₂ conversion (%) and selectivity for the ionic liquid catalysts at 20 bar and 45 mL/min corresponding to a space velocity of 5400 mL/h/gcat.

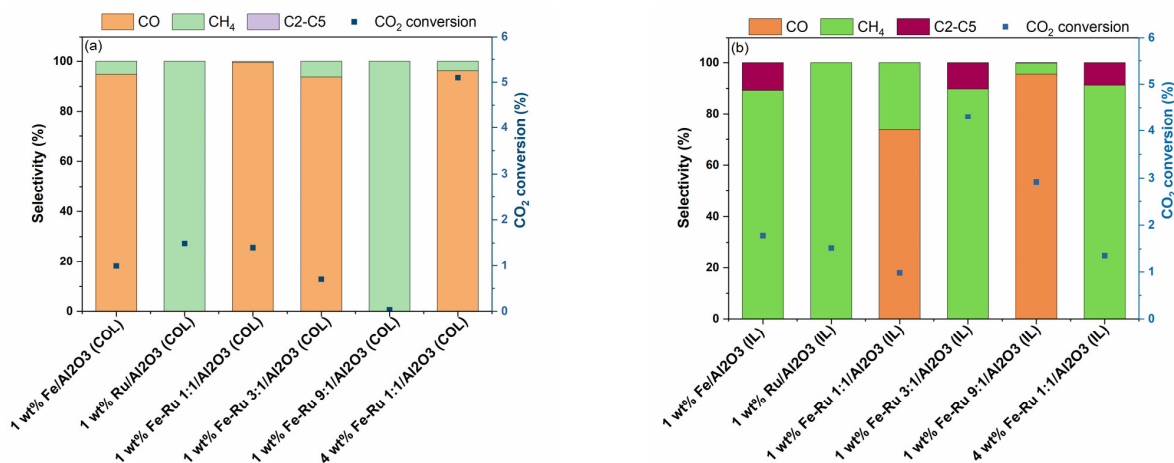


Figure 5. (a) CO₂ conversion (%) and selectivity of the colloidal catalysts at 20 bar and 15 mL/min corresponding to a space velocity of 1800 mL/h/gcat. (b) CO₂ conversion (%) and selectivity of the ionic liquid catalysts at 20 bar and 15 mL/min corresponding to a space velocity of 1800 mL/h/gcat.

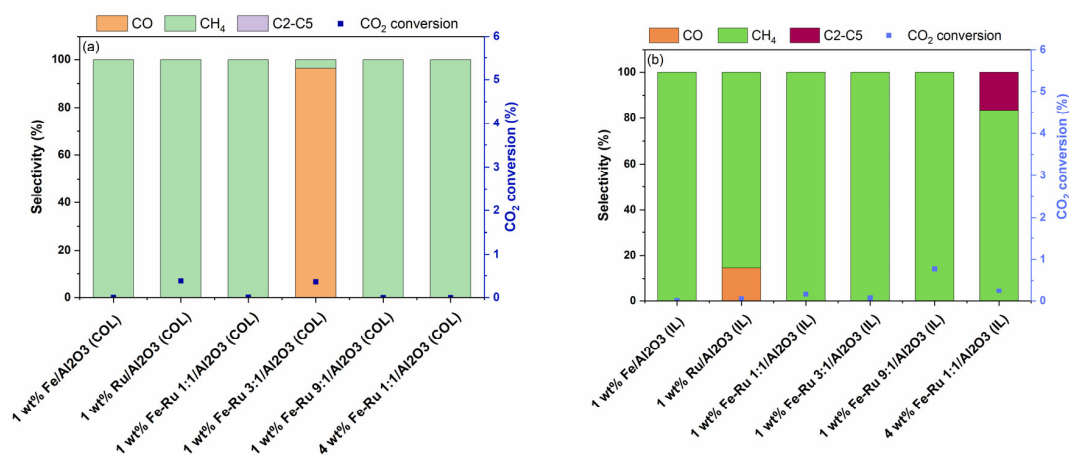


Figure 6. (a) CO₂ conversion (%) and selectivity of the colloidal catalysts at 6 bar and 45 mL/min corresponding to a space velocity of 5400 mL/h/gcat. (b) CO₂ conversion (%) and selectivity of the ionic liquid catalysts at 6 bar and 45 mL/min corresponding to a space velocity of 5400 mL/h/gcat.

The results of activity tests in the hydrogenation of CO₂ at 20 bar total pressure and 45 mL/min are summarized in Figure 4.

As shown in Figure 4a for COL samples and Figure 4b for IL samples, when using 1 wt.% Fe/Al₂O₃ catalysts prepared using COL and IL synthesis methods, distinct selectivity profile was observed. When using 1 wt.% Fe/Al₂O₃ (COL) catalyst, CO was obtained as the major product, while when using 1 wt.% Fe/Al₂O₃ (IL) catalyst, selectivity shifted from CO to CH₄ and C₂–C₅ hydrocarbons. However, the 1 wt.% Ru/Al₂O₃ catalysts prepared using both COL and IL synthesis methods showed similar product profiles with 100% selectivity to CH₄. When comparing the bimetallic 1 wt.% Fe–Ru 1:1/Al₂O₃ catalysts, while COL catalyst showed high selectivity to CO, the IL catalyst showed a shift in product selectivity, resulting in the mixture of CO and CH₄. The observed shift in product selectivity was more prominent when the total metal loading was increased from 1 wt.% to 4 wt.%. While the 4 wt.% Fe–Ru 1:1/Al₂O₃ (COL) catalyst showed CO as the major product, the 4 wt.% Fe–Ru 1:1/Al₂O₃ (IL) catalyst showed CH₄ and C₂–C₅ hydrocarbons as major products.

It is widely acknowledged that CO₂ is reduced to CO via the RWGS reaction on the Fe₃O₄ active sites, while the presence of Fe₅C₂ facilitates the FT reaction for the formation of hydrocarbons. To investigate the influence of the catalyst synthesis method on the formation of active sites, we further carried out the XRD characterization of the spent catalysts prepared by both COL and IL methods (Figure S1). For instance, the 1 wt.% Fe–Ru 1:1/Al₂O₃ (COL) catalyst (Figure S1a) indicated the presence of Fe₂O₃ and Fe₃O₄, while both 1 wt.% Fe/Al₂O₃ (IL) and 1 wt.% Fe–Ru 1:1/Al₂O₃ (IL) catalysts clearly depicted the presence of Fe₅C₂, indicating that Fe₃O₄ was fully carburized to Fe₅C₂. It is worth noting that this iron carbide phase plays a key role in the subsequent C–C chain growth reaction. Thus, it is noticeable that the catalyst synthesis method has a strong influence on the ultimate structure of the catalyst active sites. From the structure–activity correlation determined from the XRD analysis of fresh and spent catalysts and observed product selectivity profiles, it is noticeable that the ionic liquid synthesis method facilitates the formation of Fe₅C₂ species, which facilitate the FT reaction, promoting the formation of C₂–C₅ hydrocarbons.

The influence of space velocity at 20 bar total pressure was evaluated by performing the hydrogenation of CO₂ at 15 mL/min, and the results are summarized in Figure 5.

As shown in Figure 5a,b, when using 1 wt.% Fe/Al₂O₃ catalysts prepared using the COL and IL synthesis methods at 1800 mL/h/gcat, a similar shift in selectivity profile was observed, as seen previously at 5400 mL/h/gcat (Figure 4), albeit higher CO₂ conversions were observed at lower GHSV values, which is expected due to the increased residence time. When comparing the bimetallic 1 wt.% Fe–Ru 1:1/Al₂O₃ catalysts, higher CH₄ and C₂–C₅ hydrocarbon selectivity values were observed with the catalyst synthesized using the IL method. Amongst the bimetallic catalysts, 1 wt.% Fe–Ru 3:1/Al₂O₃ (IL) showed the highest conversion and C₂–C₅ hydrocarbon selectivity, indicating the most optimal catalytic performance.

The effect of total pressure on the product selectivity was evaluated via the hydrogenation of CO₂ at 6 bar pressure and 5400 mL/h/gcat. The results of activity tests at 6 bar and 45 mL/min are summarized in Figure 6.

As shown in Figure 6a,b, when using 1 wt.% Fe/Al₂O₃ catalysts prepared using both COL and IL synthesis methods at 6 bar total pressure, 100% selectivity to CH₄ was observed, albeit with lower CO₂ conversions. Similarly, bimetallic 1 wt.% Fe–Ru 1:1/Al₂O₃ catalysts prepared using both COL and IL methods displayed similarly high CH₄ selectivity. While the 4 wt.% Fe–Ru 1:1/Al₂O₃ (COL) catalyst showed CH₄ as the only product, the 4 wt.% Fe–Ru 1:1/Al₂O₃ (IL) catalyst showed CH₄ as major product, with excellent hydrocarbons selectivity of 16.5% to C₂–C₅, and 83.5% selectivity to CH₄.

3. Materials and Methods

3.1. Materials

Triruthenium dodecacarbonyl ($\text{Ru}_3(\text{CO})_{12}$, 99%), Tris(acetylacetonato)iron(III) ($\text{Fe}(\text{acac})_3$, 97%), Iron(0) carbonyl ($\text{Fe}(\text{CO})_5$, >99.99%), 1-oleylamine (OLAM, 90%), and 1-octadecene (ODE, 99%) were purchased from Merck (Darmstadt, Germany), and oleic acid (OLAC, 99%) was purchased from Thermo Scientific Chemicals™ (Waltham, MA USA). The alumina used as support was $\gamma\text{-Al}_2\text{O}_3$ (S.A. 100 m^2/g , 99.9%), purchased from Thermo Scientific Chemicals. All solvents were of analytical HPLC grade and all reagents were used as received. All calcined supports and samples were ground and sieved below 180 μm grain size.

3.2. Synthesis of NPs

Ru nanoparticles were synthesized via colloidal synthesis by the thermal decomposition of $\text{Ru}_3(\text{CO})_{12}$ using a standard Schlenk technique with slight modifications (Aitbekova et al., 2019) [11]. In a 2-neck flask, 100 mg of $\text{Ru}_3(\text{CO})_{12}$ and 20 mL of oleylamine were combined, degassed under vacuum and argon, heated to 270 °C, and maintained for 30 min. After cooling and adding 15 mL of ethanol, the nanoparticles were isolated by centrifugation at 4400 rpm for 3 min and dispersed in 10 mL of hexane. Fe nanoparticles were prepared following the same protocol, using 10 mL of oleylamine and 1 mmol of $\text{Fe}(\text{acac})_3$, dehydrated at 110 °C, rapidly heated to 300 °C, and aged for 1 h. After washing with ethanol, the solid metal nanoparticles were recovered and dispersed in 10 mL of hexane. Bimetallic Ru–Fe nanoparticles were synthesized from a hexane solution containing previously prepared ruthenium nanoparticles, along with 1-octadecene (ODE), oleic acid (OLAC), and oleylamine (OLAM). After degassing for 30 min at 120 °C under a continuous flow of nitrogen and the careful injection of $\text{Fe}(\text{CO})_5$, the mixture was heated to 300 °C for 30 min. Following two washing steps, initially with isopropyl alcohol, followed by dispersion in 5 mL of hexane, and then with the addition of 10 mL of ethanol, the nanoparticles were separated through centrifugation (4400 rpm for 3 min) and dispersed in hexane.

In the ionic liquid (IL)-assisted method for synthesizing nanoparticles, 5 g of $[\text{BmIm}][\text{BF}_4]$ and 337 mg of $\text{Fe}(\text{acac})_3$ (for Fe oxide NPs) or 105 g of $\text{Ru}_3(\text{CO})_{12}$ (for Ru NPs) were utilized in separate reactions. For the Fe oxide NPs, the mixture was heated to 200 °C for 16 h under argon, followed by the addition of 20 mL of ethanol for nanoparticle separation through centrifugation at 8000 rpm. The isolated iron oxide nanoparticles were then dispersed in 15 mL of ethanol. Similarly, for Ru NPs, the solution was maintained at 250 °C for 18 h, and after adding 15 mL of ethanol, the particles were separated via centrifugation and redispersed in 15 mL of ethanol.

For the bimetallic Fe–Ru NPs, three different molar ratios were examined: 1:1, 3:1 and 9:1. In all cases, a controlled environment within a glove box was used, with $\text{Fe}(\text{acac})_3$ and $\text{Ru}_3(\text{CO})_{12}$ meticulously introduced into $[\text{BmIm}][\text{PF}_6]$. After undergoing appropriate reductions at 250 °C for 18 h, the resulting nanoparticles were deposited onto the support material. For the 1:1 ratio, 95 mg of $\text{Fe}(\text{acac})_3$ and 65 mg of $\text{Ru}_3(\text{CO})_{12}$ were employed, while for the 3:1 ratio, approximately 106.5 mg of $\text{Fe}(\text{acac})_3$ and approximately 23 mg of $\text{Ru}_3(\text{CO})_{12}$ were used. Finally, for the 9:1 Fe–Ru NPs, 152 mg of iron precursor and 12 mg of ruthenium precursor were mixed with 3 g of ionic liquid, and the solution was heated to 200 °C for 18 h before direct deposition onto the support material. This approach aimed to minimize nanoparticle aggregation during dispersion in polar solvents, and to ensure effective deposition on the alumina support.

3.3. Catalyst Preparation

In the colloidal method for supporting nanoparticles on $\gamma\text{-Al}_2\text{O}_3$, both Fe and Ru NPs were prepared similarly. An appropriate quantity of different types of NPs was added to the $\gamma\text{-Al}_2\text{O}_3$ support dispersed in hexanes under vigorous stirring (30 min at 1400 rpm) to achieve a total metal loading of 1 or 4 wt.%. Afterward, centrifugation at 4000 rpm for 3 min separated the solid phase, which was then dried at 80 °C for 4 h to eliminate

organic residues and sieved using a 150 μm sieve. Additionally, for the preparation of Ru–Fe oxide NPs on $\gamma\text{-Al}_2\text{O}_3$, TGA analysis indicated a yield of 5.1 mg (Fe + Ru)/mL, requiring approximately 4 mL of solution to introduce 20 mg of metal (1% relative to 2 g of $\gamma\text{-Al}_2\text{O}_3$). The subsequent steps of the procedure were consistent with those employed for Fe and Ru NPs, involving hexane addition, agitation, centrifugation, drying, and sieving using the same mesh size.

Regarding the supporting method on $\gamma\text{-Al}_2\text{O}_3$ for catalysts synthesized with ionic liquids (ILs), the IL with dispersed metallic NPs solution was cooled to 75 $^\circ\text{C}$ to increase the ionic liquid's viscosity. Subsequently, 10 mL of ethanol was added, and the solution underwent centrifugation for 10 min at 8000 rpm to separate the solid NPs from the liquid phase. After several washes with ethanol, the particles were deposited in a mortar. Following the addition of the desired amount of alumina, the powder was mechanically agitated and ground for 15–20 min to achieve a uniform color and metal distribution. Finally, the resulting catalyst was dried at 80 $^\circ\text{C}$ to remove residual organics and calcined to complete the process.

All the obtained catalysts are reported in Table 1, detailing the synthetic method, the total metal loading, and the Fe:Ru ratio

3.4. Catalyst Characterization

X-ray fluorescence (XRF) spectroscopy (Horiba, Kyoto, Japan) was used to determine the elemental composition of the catalysts prepared with colloidal and ionic liquid synthesis. Table 1 shows the actual composition of each element compared to the calculated amount.

The textural properties of the synthesized samples have been determined by N_2 adsorption–desorption isotherms measured at -196 $^\circ\text{C}$ using the Micromeritics Tristar 3000 instrument (Norcross, GA, USA). Prior to the analysis, the samples were evacuated at 120 $^\circ\text{C}$ for 3 h.

Powder X-ray diffraction (XRD) (Rigaku, Tokyo, Japan) analysis of the fresh and spent catalysts was carried out using a D8 Advance Bruker[®] diffractometer (Billerica, MA, USA) with $\text{Cu-K}\alpha$ radiation, $\lambda = 1.5405$ \AA . The measurements were taken from 20 to 90 degrees (2θ) at a scan rate of 0.01 $^\circ$ per step and a scan time of 0.5 s^{-1} per step.

The reducibility of calcined FeRu catalysts was investigated by the temperature programmed reduction (TPR) technique in H_2 ($\text{H}_2\text{-TPR}$). In a typical test, the powdered catalyst was placed in a quartz reactor and, after a pre-treatment in flowing 10% O_2/He (35 mL/min) carried out by heating from ambient temperature to 500 $^\circ\text{C}$ at a rate of 20 $^\circ\text{C}/\text{min}$, was cooled down to -10 $^\circ\text{C}$. Then, the flow was switched to 5 vol.% H_2 in Ar at 53 mL/min and the reactor temperature was increased to 900 $^\circ\text{C}$ at 10 $^\circ\text{C}/\text{min}$. Hydrogen consumption was monitored by a thermal conductivity detector (TCD) placed downstream of the reactor, after a cold trap.

Scanning electron microscopy (SEM) analysis was performed using FEI Quanta FEG 200 environmental SEM (Hillsboro, OR, USA) in a high-vacuum mode with EDX accessories attached. Prior to the measurement, the sample in powder form was sprinkled on carbon tape (adhesive) and mounted on the SEM sample holder.

3.5. Catalytic Activity Testing

Activity tests were carried out in a lab-scale plant equipped with a fixed-bed reactor. Approximately 500 mg of catalyst powder was diluted with Al_2O_3 in a 1:10 dilution ratio, and this was physically mixed and loaded into the reactor between two layers of quartz wool. The reactor was heated using a Carbolite-Gero MTF single zone tube furnace (Derbyshire, UK) while the catalyst bed temperature was measured using a K-type thermocouple inserted in the middle of the reactor bed. The reaction mixture consisted of 3:1 $\text{H}_2:\text{CO}_2$. Kinetic experiments were conducted at 320 $^\circ\text{C}$, and at 6 and 20 bar total pressure with a gas-hourly space velocity (GHSV) of 5400 mL/h/gcat. Catalytic tests were also repeated at the same temperature, 320 $^\circ\text{C}$, at 20 bar total pressure and a GHSV of 1800 mL/h/gcat, to assess the effect of spatial velocity on the catalyst performance.

Prior to catalytic activity testing, each catalyst was pretreated in pure H₂ at 400 °C for 5 h with a temperature ramp rate of 2 °C min⁻¹. The outlet reactor stream was analyzed to determine CO₂ conversion and product selectivity using a GC (Agilent, 8860, Santa Clara, CA, USA) equipped with a TCD detector connected to a packed column along with a FID detector connected to CP-Sil PONA column along with a FT-IR gas analyzer (Bruker[®], MATRIX-MG5, Billerica, MA, USA).

4. Conclusions

This study presents an innovative approach to synthesizing bimetallic catalysts based on iron (Fe) and ruthenium (Ru) by utilizing ionic liquids as solvents. These bimetallic catalysts leverage the synergistic interaction between the two metals, resulting in enhanced performance in the direct hydrogenation of CO₂ with increased selectivity towards light hydrocarbons in the LPG range (C₂–C₅). Significantly, at 20 bar pressure, 5400 mL/h/gcat, and 320 °C, both monometallic 1% Fe and bimetallic 1% Fe–Ru 1:1 catalysts, prepared using the newly developed ionic liquids (IL) method, exhibited selectivity towards C₂–C₅ hydrocarbons in CO₂ hydrogenation, contrary to the catalyst with the same composition prepared with the colloidal method that demonstrated selectivity towards CO and methane. This shift in product selectivity becomes even more prominent with a decrease in space velocity from 5400 to 1800 mL/h/gcat. Elevating the overall metal loading to 4 wt.% in the Fe–Ru 1:1 IL catalyst resulted in a significant rise in the generation of C₂–C₅ hydrocarbons, exhibiting a selectivity of 16.5% for C₂–C₅ and 83.5% for CH₄. Under low-pressure conditions (6 bar), a shift in selectivity from CO to methane in the catalysts synthesized with IL solvents was also observed, despite the limitations imposed on product selectivity by the moderate pressure. This shift in product selectivity is intricately linked to the synergistic interplay between iron and ruthenium observed in the IL catalysts, as evidenced by the distinct reduction profiles observed in H₂-TPR experiments. Further support is derived from the analysis of the spent catalyst using XRD, which establishes a correlation between CO₂ hydrogenation to hydrocarbons via the Fischer–Tropsch route and the presence of iron carbide species on the IL catalyst surface—the active phases for the reaction.

In conclusion, this study successfully demonstrates the enhanced cooperativity between bimetallic Fe and Ru species synthesized using the IL method, resulting in superior activity and selectivity towards LPG-range hydrocarbons compared to the classical colloidal synthesis method. This work marks a significant advancement in the field and holds the potential to contribute to sustainable energy solutions, including the conversion of CO₂ into net-zero e-fuels for the transport sector and the development of renewable resources using CO₂ as a carbon feedstock.

Supplementary Materials: The following supporting information can be downloaded at: <https://www.mdpi.com/article/10.3390/catal13121499/s1>, Figure S1: (a) XRD patterns of spent catalysts 1 wt.% Fe–Ru 1:1/Al₂O₃ (COL) (in violet), 1 wt.% Fe–Ru 3:1/Al₂O₃ (COL) (in orange) and 1 wt.% Fe–Ru 3:1/Al₂O₃ (COL) (in light blue), compared with the pure γ -Al₂O₃. (b) XRD patterns of spent catalysts, 1 wt.% Fe₂O₃/Al₂O₃ (IL) (in violet), 1 wt.% Fe–Ru 1:1/Al₂O₃ (IL) (in blue), 1 wt.% Fe–Ru 3:1/Al₂O₃ (IL) (in red) and 1 wt.% Fe–Ru 9:1/Al₂O₃ (IL) (in green), compared with the pure γ -Al₂O₃.

Author Contributions: M.M.: methodology, formal analysis, resources, data curation, writing—original draft preparation, visualization, A.C.-P.: methodology, formal analysis, investigation, data curation, writing—review and editing, visualization, S.A.: formal analysis, investigation, data curation, visualization, N.J.M.: formal analysis, investigation, data curation, visualization, H.M.: conceptualization, methodology, validation, resources, data curation, writing—review and editing, funding acquisition, supervision N.A.: conceptualization, methodology, validation, resources, data curation, writing—original draft preparation, funding acquisition, project administration, supervision. All authors have read and agreed to the published version of the manuscript.

Funding: The authors gratefully acknowledge the European Union—NextGenerationEU—for funding PROMETH₂eus project—ID RSH2A_000039. The authors are also thankful for the financial support for Ph.D. studentship given to N.J.M. funded by Queen’s University Belfast and Tezpur University India. H.M. thankfully acknowledges the funding and support provided by the Leverhulme Trust research grant RPG-2020-301, as well as the UK Catalysis hub via our membership of the UK Catalysis Hub Consortium funded by EPSRC grant: EP/R026645/1.

Data Availability Statement: The data presented in this study are available in the article.

Conflicts of Interest: The authors declare no conflict of interest.

References

1. IPCC. *Global Warming of 1.5 °C*; IPCC: Geneva, Switzerland, 2022.
2. European LPG Association. *Autogas in Europe, the Sustainable Alternative: An LPG Industry Roadmap*; AEGPL: Brussels, Belgium, 2013.
3. Raslavičius, L.; Keršys, A.; Mockus, S.; Keršiene, N.; Starevičius, M. Liquefied Petroleum Gas (LPG) as a Medium-Term Option in the Transition to Sustainable Fuels and Transport. *Renew. Sustain. Energy Rev.* **2014**, *32*, 513–525. [[CrossRef](#)]
4. Ashok, B.; Denis Ashok, S.; Ramesh Kumar, C. LPG Diesel Dual Fuel Engine—A Critical Review. *Alex. Eng. J.* **2015**, *54*, 105–126. [[CrossRef](#)]
5. Lietti, L.; Righini, L.; Castoldi, L.; Artioli, N.; Forzatti, P. Labeled ¹⁵N₂ study on N₂ and N₂O formation over Pt-Ba/Al₂O₃ NSR catalysts. *Top. Catal.* **2013**, *56*, 7–13. [[CrossRef](#)]
6. Porosoff, M.D.; Yan, B.; Chen, J.G. Catalytic Reduction of CO₂ by H₂ for Synthesis of CO, Methanol and Hydrocarbons: Challenges and Opportunities. *Energy Environ. Sci.* **2016**, *9*, 62–73. [[CrossRef](#)]
7. Dorner, R.W.; Hardy, D.R.; Williams, F.W.; Willauer, H.D. Heterogeneous Catalytic CO₂ Conversion to Value-Added Hydrocarbons. *Energy Environ. Sci.* **2010**, *3*, 884–890. [[CrossRef](#)]
8. Coney, C.; Hardacre, C.; Morgan, K.; Artioli, N.; York, A.P.E.; Millington, P.; Kolpin, A.; Goguet, A. Investigation of the oxygen storage capacity behaviour of three way catalysts using spatio-temporal analysis. *Appl. Catal. B.* **2019**, *258*, 117918. [[CrossRef](#)]
9. Riedel, T.; Claeys, M.; Schulz, H.; Schaub, G.; Nam, S.S.; Jun, K.W.; Choi, M.J.; Kishan, G.; Lee, K.W. Comparative Study of Fischer-Tropsch Synthesis with H₂/CO and H₂/CO₂ Syngas Using Fe- and Co-Based Catalysts. *Appl. Catal. A Gen.* **1999**, *186*, 201–213. [[CrossRef](#)]
10. Meffre, A.; Iablokov, V.; Xiang, Y.; Barbosa, R.; Fazzini, P.F.; Kelsen, V.; Kruse, N.; Chaudret, B. Influence of Chemical Composition on the Catalytic Activity of Small Bimetallic FeRu Nanoparticles for Fischer-Tropsch Syntheses. *Catal. Lett.* **2015**, *145*, 373–379. [[CrossRef](#)]
11. Aitbekova, A.; Goodman, E.D.; Wu, L.; Boubnov, A.; Hoffman, A.S.; Genc, A.; Cheng, H.; Casalena, L.; Bare, S.R.; Cargnello, M. Engineering of Ruthenium-Iron Oxide Colloidal Heterostructures: Improved Yields in CO₂ Hydrogenation to Hydrocarbons. *Angew. Chem.—Int. Ed.* **2019**, *58*, 17451–17457. [[CrossRef](#)]
12. Lee, S.C.; Jang, J.H.; Lee, B.Y.; Kim, J.S.; Kang, M.; Lee, S.B.; Choi, M.J.; Choung, S.J. Promotion of Hydrocarbon Selectivity in CO₂ Hydrogenation by Ru Component. *J. Mol. Catal. A Chem.* **2003**, *210*, 131–141. [[CrossRef](#)]
13. Jiang, F.; Liu, B.; Geng, S.; Xu, Y.; Liu, X. Hydrogenation of CO₂ into Hydrocarbons: Enhanced Catalytic Activity over Fe-Based Fischer-Tropsch Catalysts. *Catal. Sci. Technol.* **2018**, *8*, 4097–4107. [[CrossRef](#)]
14. Krämer, J.; Redel, E.; Thomann, R.; Janiak, C. Use of Ionic Liquids for the Synthesis of Iron, Ruthenium, and Osmium Nanoparticles from Their Metal Carbonyl Precursors. *Organometallics* **2008**, *27*, 1976–1978. [[CrossRef](#)]
15. Kunz, W.; Häckl, K. The Hype with Ionic Liquids as Solvents. *Chem. Phys. Lett.* **2016**, *661*, 6–12. [[CrossRef](#)]
16. Kaur, G.; Kumar, H.; Singla, M. Diverse Applications of Ionic Liquids: A Comprehensive Review. *J. Mol. Liq.* **2022**, *351*, 118556. [[CrossRef](#)]
17. Castoldi, L.; Matarrese, R.; Kubiak, L.; Daturi, M.; Artioli, N.; Pompa, S.; Lietti, L. In-depth insights into N₂O formation over Rh- and Pt-based LNT catalysts. *Catal. Today* **2019**, *320*, 09205861. [[CrossRef](#)]
18. Byrne, E.L.; O’Donnell, R.; Gilmore, M.; Artioli, N.; Holbrey, J.D.; Swadźba-Kwaśny, M. Hydrophobic Functional Liquids Based on Trioctylphosphine Oxide (TOPO) and Carboxylic Acids. *Phys. Chem. Chem. Phys.* **2020**, *22*, 24744–24763. [[CrossRef](#)] [[PubMed](#)]
19. Pandit, K.; Jeffrey, C.; Keogh, J.; Tiwari, M.S.; Artioli, N.; Manyar, H.G. Techno-Economic Assessment and Sensitivity Analysis of Glycerol Valorization to Biofuel Additives via Esterification. *Ind. Eng. Chem. Res.* **2023**, *62*, 9201–9210. [[CrossRef](#)]
20. Jakubek, T.; Hudy, C.; Gryboś, J.; Manyar, H.; Kotarba, A. Thermal Transformation of Birnessite (OL) Towards Highly Active Cryptomelane (OMS-2) Catalyst for Soot Oxidation. *Catal. Lett.* **2019**, *149*, 2218–2225. [[CrossRef](#)]
21. O’Donnell, R.; Ralphs, K.; Grolleau, M.; Manyar, H.; Artioli, N. Doping Manganese Oxides with Ceria and Ceria Zirconia Using a One-Pot Sol-Gel Method for Low Temperature Diesel Oxidation Catalysts. *Top. Catal.* **2020**, *63*, 351–362. [[CrossRef](#)]
22. Quan, C.; Zhang, G.; Gao, N.; Su, S.; Artioli, N.; Feng, D. Behavior Study of Migration and Transformation of Heavy Metals during Oily Sludge Pyrolysis. *Energy Fuels* **2022**, *36*, 8311–8322. [[CrossRef](#)]
23. Ethiraj, J.; Wagh, D.; Manyar, H. Advances in Upgrading Biomass to Biofuels and Oxygenated Fuel Additives Using Metal Oxide Catalysts. *Energy Fuels* **2022**, *36*, 1189–1204. [[CrossRef](#)]

24. Mazumdar, N.J.; Kumar, P.; Arredondo-Arechavala, M.; Artioli, N.; Manyar, H. Intensifying levulinic acid hydrogenation using mechanochemically prepared copper on manganese oxide catalysts. *Chem. Eng. J.* **2023**, *478*, 147479. [[CrossRef](#)]
25. Keogh, J.; Deshmukh, G.; Manyar, H. Green Synthesis of Glycerol Carbonate via Transesterification of Glycerol Using Mechanochemically Prepared Sodium Aluminate Catalysts. *Fuel* **2022**, *310*, 122484. [[CrossRef](#)]
26. Wang, H.; Ning, P.; Zhang, Q.; Liu, X.; Zhang, T.; Fan, J.; Wang, J.; Long, K. Promotional Mechanism of WO_3 over $\text{RuO}_2\text{-Fe}_2\text{O}_3$ Catalyst for $\text{NH}_3\text{-SCO}$ Reaction. *Appl. Catal. A Gen.* **2018**, *561*, 158–167. [[CrossRef](#)]
27. Tian-Yu, G.; Liu, S.-Y.; Qing, M.; Feng, J.-L.; Zhen-Gang, L.Ü.; Wang, H.; Yong, Y. In Situ XRD Study of the Effect of H_2O on Fe_5C_2 Phase and Fischer-Tropsch Performance. *J. Fuel Chem. Technol.* **2020**, *48*, 75–82.
28. Wang, H.M.; Ning, P.; Zhang, Q.L.; Liu, X.; Zhang, T.X.; Hu, J.; Wang, L.Y. Effect of Different RuO_2 Contents on Selective Catalytic Oxidation of Ammonia over $\text{RuO}_2\text{-Fe}_2\text{O}_3$ Catalysts. *Ranliao Huaxue Xuebao/J. Fuel Chem. Technol.* **2019**, *47*, 215–223. [[CrossRef](#)]
29. Fukushima, T.; Arakawa, H.; Ichikawa, M. In Situ High-Pressure FT-IR Studies on the Surface Species Formed in CO Hydrogenation on SiO_2 -Supported Rh-Fe Catalysts. *J. Phys. Chem.* **1985**, *89*, 4440–4443. [[CrossRef](#)]
30. Liu, J.; Zhang, G.; Jiang, X.; Wang, J.; Song, C.; Guo, X. Insight into the Role of Fe_5C_2 in CO_2 Catalytic Hydrogenation to Hydrocarbons. *Catal. Today* **2021**, *371*, 162–170. [[CrossRef](#)]
31. Lin, Q.; Cheng, M.; Zhang, K.; Li, W.; Wu, P.; Chang, H.; Lv, Y.; Men, Z. Development of an Iron-Based Fischer-Tropsch Catalyst with High Attrition Resistance and Stability for Industrial Application. *Catalysts* **2021**, *11*, 908. [[CrossRef](#)]
32. Li, F.; Qian, W. DRIFTS Study of Fe Promoter Effect on Rh/ Al_2O_3 Catalyst for C_2 Oxygenates Synthesis from Syngas. *Appl. Petrochem. Res.* **2019**, *9*, 211–219. [[CrossRef](#)]

Disclaimer/Publisher's Note: The statements, opinions and data contained in all publications are solely those of the individual author(s) and contributor(s) and not of MDPI and/or the editor(s). MDPI and/or the editor(s) disclaim responsibility for any injury to people or property resulting from any ideas, methods, instructions or products referred to in the content.